Tangential-normal surface testing for the nonconforming discretization of the Electric-Field Integral Equation

E. Ubeda, I. Sekulic, Juan M. Rius and A. Heldring

Abstract—**Nonconforming implementations of the Electric-Field Integral Equation (EFIE), based on the facet-oriented monopolar-RWG set, impose no continuity constraints in the expansion of the current between adjacent facets. These schemes become more versatile than the traditional edge-oriented schemes, based on the RWG set, because they simplify the management of junctions in composite objects and allow the analysis of nonconformal triangulations. Moreover, for closed moderately small conductors with edges and corners, they show improved accuracy with respect to the conventional RWG-discretization. However, they lead to elaborate numerical schemes because the fields are tested inside the body, near the boundary surface, over volumetric subdomains attached to the surface meshing. In this paper, we present a new nonconforming discretization of the EFIE that results from testing with RWG functions over pairs of triangles such that one triangle matches one facet of the surface triangulation and the other one is oriented perpendicularly, inside the body. This "tangential-normal" testing scheme, based on surface integrals, simplifies considerably the matrix generation when compared with the volumetrically tested approaches.**

Index Terms—**Basis functions, electric field integral equation (EFIE), integral equations, moment method**

I. INTRODUCTION

TRADITIONAL Method-of-Moment (MoM) schemes of discretization of the Electric-Field Integral Equation (EFIE) rely on divergence-conforming sets, such as the RWG set, which impose the normal continuity of the current across the edges arising from the discretization [1][2]. The resulting numerical implementations are little demanding in computational terms because the hypersingular Kernel contributions are cancelled out [2]. Recently, nonconforming schemes based on the facet-oriented monopolar-RWG set [3], with no interelement continuity constraint, have been developed for the discretization of the EFIE in the EM scattering analysis of closed conductors [4][5]. These implementations carry out the numerical evaluation of the hypersingular Kernel contributions by testing the fields over volumetric subdomains inside the body, tetrahedral elements [4] or wedges [5], attached to the surface triangulation. However, the generation of the impedance matrix elements becomes rather elaborate and more time-consuming than the conventional surface-tested Galerkin RWG-discretization. In

this paper, we present a new nonconforming discretization of the EFIE with an RWG-based testing scheme, defined over pairs of connected triangles. We call this scheme "tangential-normal" because one triangle, tangential to the boundary, matches a particular surface facet in the surface triangulation and the other triangle is oriented normally to the boundary surface, into the body. This nonconforming implementation simplifies considerably the matrix generation. Furthermore, the resulting impedance matrix, unlike the previous volumetrically tested schemes, can be made immune to the low-frequency breakdown through an easy-to-implement algebraic manipulation.

II. TANGENTIAL-NORMAL SURFACE TESTING

The monopolar-RWG set is defined like the RWG set inside facets but with no normal-continuity constraint across edges. Therefore, this set arises from grouping two subsets of basis functions, $\left\{f_n^1\right\}$, $\left\{f_n^2\right\}$, associated with the two triangles at both sides of the Ne edges arising from the triangulation. The unnormalized definition of these functions becomes

$$f_n^i(r) = \frac{1}{2A_n^i}\left(r - r_n^i\right) \qquad i = 1, 2 \quad n = 1..Ne \qquad (1)$$

where r_n^1, r_n^2 denote the two opposed vertices to the nth edge and A_n^1, A_n^2 stand for the areas of T_n^1, T_n^2, the corresponding triangles at both sides of the nth edge.

The approximated scattered field at the point r arising from the monopolar-RWG expansion of the current becomes

$$\tilde{E}^s(r) = -jk\eta_0 \sum_{i=1}^{2}\sum_{n=1}^{Ne} c_n^i \iint_{T_n^i} G(r,r') f_n^i(r') ds'$$

$$-\sum_{i=1}^{2}\sum_{n=1}^{Ne} c_n^i \nabla \Phi_n^i(r) \qquad (2)$$

where $\left\{c_n^1\right\}, \left\{c_n^2\right\}$ denote the subsets of unknowns and G, k, η_0 represent, respectively, the free-space Green's function, the wavenumber and the free-space impedance. The terms Φ_n^1, Φ_n^2 stand for the nth-edge monopolar-RWG contributions in the expansion of the scalar potential, which are defined as [4]

$$\Phi_n^i(\mathbf{r}) = j\frac{\eta_0}{k}\iint_{T_n^i} G(\mathbf{r},\mathbf{r}')\nabla'\cdot\mathbf{f}_n^i ds'$$

$$- j\frac{\eta_0}{k}\oint_{\partial T_n^i} G(\mathbf{r},\mathbf{r}')\left(\mathbf{f}_n^i\cdot\mathbf{n}_{c,n}^i\right)dl' \quad i=1,2 \; n=1..Ne \tag{3}$$

where ∂T_n^1, ∂T_n^2 denote the closed line contours, respectively, around T_n^1, T_n^2. The unit vectors $\mathbf{n}_{c,n}^1$, $\mathbf{n}_{c,n}^2$ are perpendicular to these contours (see Fig. 1).

The tangential-normal scheme of testing leads to the following expression

$$\int_{T_m^p\cup T_m^N} \mathbf{E}^i\cdot\mathbf{R}_m^p ds = -\int_{T_m^p\cup T_m^N}\tilde{\mathbf{E}}^s\cdot\mathbf{R}_m^p ds \quad p=1,2 \; m=1..Ne \tag{4}$$

where $\mathbf{E}^i$ stands for the incident electric field and $\mathbf{R}_m^1$, $\mathbf{R}_m^2$ denote RWG functions that straddle each of the two surface triangles T_m^1, T_m^2 at the mth edge, and T_m^N, the isosceles triangle that evolves from the mth edge into the body over the direction resulting from averaging the normal directions at the adjacent facets (see Fig. 1). The testing functions in (4), which we name "tangential-normal", are defined as

$$\mathbf{R}_m^p(\mathbf{r}) = \begin{cases} \mathbf{f}_m^p(\mathbf{r}) & \mathbf{r}\in T_m^p \\ -\mathbf{g}_m(\mathbf{r}) & \mathbf{r}\in T_m^N \end{cases} \quad p=1,2 \; m=1..Ne \tag{5}$$

such that $\mathbf{g}_m(\mathbf{r})$ yields

$$\mathbf{g}_m(\mathbf{r}) = \frac{1}{2A_m^N}\left(\mathbf{r}-\mathbf{r}_m^N\right) \quad m=1..Ne \tag{6}$$

where $\mathbf{r}_m^N$ represents the vertex in T_m^N opposed to the mth edge and A_m^N denotes the area of T_m^N.

The tangential-normal monopolar-RWG discretization of the EFIE gives rise to the following matrix system

$$E_m^{i,p} = \sum_{i=1}^{2}\sum_{n=1}^{Ne} Z_{mn}^{p,i}c_n^i \quad p=1,2 \; m=1..Ne \tag{7}$$

where, unlike the previous volumetrically tested schemes, the excitation vector and matrix impedance elements are now computed with surface integrals, so that, in view of (4),

$$E_m^{i,p} = \iint_{T_m^p}\mathbf{E}^i\cdot\mathbf{f}_m^p(\mathbf{r})ds - \iint_{T_m^N}\mathbf{E}^i\cdot\mathbf{g}_m^N(\mathbf{r})ds \tag{8}$$

$$Z_{mn}^{p,i} = jk\eta_0\iint_{T_m^p\cup T_m^N}\mathbf{R}_m^p(\mathbf{r})\cdot\iint_{T_n^i}G(\mathbf{r},\mathbf{r}')\mathbf{f}_n^i(\mathbf{r}')ds'ds$$

$$+ \iint_{T_m^p\cup T_m^N}\mathbf{R}_m^p(\mathbf{r})\cdot\nabla\Phi_n(\mathbf{r})ds \tag{9}$$

Thanks to the normal continuity across edges of the tangential-normal testing functions, the scalar-potential contribution in (9) is simplified so that

$$\iint_{T_m^p\cup T_m^N}\mathbf{R}_m^p(\mathbf{r})\cdot\nabla\Phi_n(\mathbf{r})ds = -\iint_{T_m^p\cup T_m^N}\nabla\cdot\mathbf{R}_m^p(\mathbf{r})\Phi_n(\mathbf{r})ds \tag{10}$$

and, in view of (3), yields

$$-j\frac{\eta_0}{k}\iint_{T_m^p\cup T_m^N}\nabla\cdot\mathbf{R}_m^p(\mathbf{r})\iint_{T_n^i}G(\mathbf{r},\mathbf{r}')\nabla'\cdot\mathbf{f}_n^i ds'ds$$

$$+j\frac{\eta_0}{k}\iint_{T_m^p\cup T_m^N}\nabla\cdot\mathbf{R}_m^p(\mathbf{r})\oint_{\partial T_n^i}G(\mathbf{r},\mathbf{r}')\left(\mathbf{f}_n^i\cdot\mathbf{n}_{c,n}^i\right)dl'ds \tag{11}$$

which becomes more compact and requires less computational effort than the analogous contributions arising from the volumetrically tested implementations [4][5].
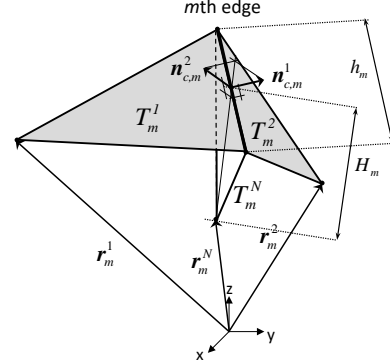
Fig. 1. T_m^1 and T_m^2 stand for the two triangles of the surface triangulation associated with the mth edge. The isosceles triangle T_m^N is defined over the plane that bisects the angle formed by T_m^1 and T_m^2.

III. LOW-FREQUENCY STABILITY

The monopolar-RWG space of current can be decomposed into two edge-oriented subspaces of current, such that the basis functions are defined in terms of the type of transition of the normal component of the current across edges [4]: (i) the divergence-conforming RWG set, $\left\{\mathbf{b}_n^e\right\}$, also called "even" monopolar-RWG set in [4][5], with continuous transition; (ii) the nonconforming "odd" monopolar-RWG set, $\left\{\mathbf{b}_n^o\right\}$, with discontinuous, odd-symmetric, transition (see Fig. 2);

$$\mathbf{b}_n^e(\mathbf{r}) = \begin{cases} +\mathbf{f}_n^1(\mathbf{r}) & \mathbf{r}\in T_n^1 \\ -\mathbf{f}_n^2(\mathbf{r}) & \mathbf{r}\in T_n^2 \end{cases} \quad n=1..Ne \tag{12}$$

$$\mathbf{b}_n^o(\mathbf{r}) = \begin{cases} +\mathbf{f}_n^1(\mathbf{r}) & \mathbf{r}\in T_n^1 \\ +\mathbf{f}_n^2(\mathbf{r}) & \mathbf{r}\in T_n^2 \end{cases} \quad n=1..Ne \tag{13}$$

Similarly, the tangential-normal testing functions in (5) can also be decomposed into two even and odd contributions, $\left\{\mathbf{t}_m^e\right\}$ and $\left\{\mathbf{t}_m^o\right\}$ at each edge, so that

$$\mathbf{t}_m^e(\mathbf{r}) = \begin{cases} +\mathbf{f}_m^1(\mathbf{r}) & \mathbf{r}\in T_m^1 \\ -\mathbf{f}_m^2(\mathbf{r}) & \mathbf{r}\in T_m^2 \end{cases} \quad m=1..Ne \tag{14}$$

$$\mathbf{t}_m^o(\mathbf{r}) = \begin{cases} +\mathbf{f}_m^1(\mathbf{r}) & \mathbf{r}\in T_m^1 \\ -2\mathbf{g}_m(\mathbf{r}) & \mathbf{r}\in T_m^N \\ +\mathbf{f}_m^2(\mathbf{r}) & \mathbf{r}\in T_m^2 \end{cases} \quad m=1..Ne \tag{15}$$

where, just like in (12), $\left\{\mathbf{t}_m^e\right\}$ also represents the RWG set.

A tangential-normal even-odd implementation of the EFIE equivalent to the development described in section II can be then defined after rearranging the source and field quantities in (1) and (5) in terms of their even and odd contributions,

which, in view of (12)-(15), result from the subtraction or summation, respectively, of the contributions at both sides of the edges. This change of testing and expansion bases involves easy-to-implement, row-wise or column-wise, algebraic manipulations. Conversely, the monopolar-RWG and tangential-normal functions at both sides (i=1,2) of the nth edge can be easily derived from their even- and odd-contributions as $(\boldsymbol{b}_n^o - (-1)^i \boldsymbol{b}_n^e)/2$ (see Fig. 2).
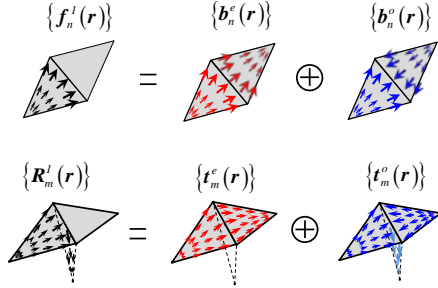
Fig. 2. Decomposition of the monopolar-RWG basis functions and tangential-normal testing functions in terms of their even and odd contributions.

The monopolar-RWG discretization of the EFIE, with tangential-normal testing, EFIE[TN][monoR], or with tetrahedral testing [4], EFIE[tet][monoR], suffers from the low-frequency breakdown (see Fig. 3). As traditionally done for the EFIE-implementations immune to the low-frequency breakdown, based on the frequency-normalized solenoidal-nonsolenoidal rearrangement of the field-testing and current-expansion subspaces, the low-frequency stable implementation of EFIE[TN][monoR], which we call EFIE[TN][Lp-St;o-monoR], is easily accomplished from the even-odd rearrangement. Indeed, the odd current-subspace generated in (13) and the tangential-to-the-surface component of the odd testing-subspace generated in (15) are nonsolenoidal [4]; the remaining RWG-subspaces, in (12) or (14), can be decomposed, as conventionally done, into the Loop, solenoidal, and Star, nonsolenoidal, contributions [6].
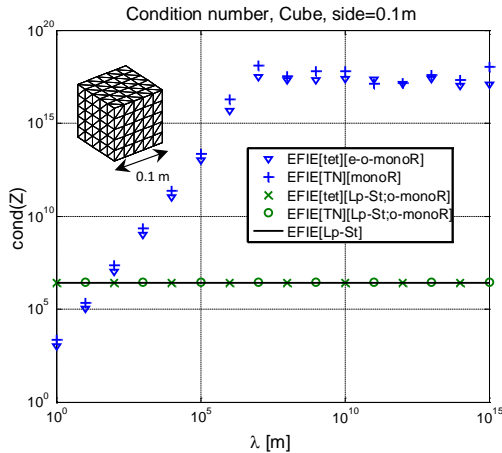
Fig. 3. Condition number over the low frequency regime of the impedance matrix resulting from the implementations EFIE[Lp-St], EFIE[TN][monoR], EFIE[tet][monoR], EFIE[TN][Lp-St;o-monoR] and EFIE[tet][Lp-St; o-monoR] for a cube with side 0.1 m and meshed with 300 triangular facets. In the monopolar-RWG implementations, H=h/10 is set.

As shown in Fig. 3, EFIE[TN][Lp-St;o-monoR] provides

stable matrix condition numbers, in similar terms as the Loop-Star discretization of the EFIE [6], EFIE[Lp-St], and the low-frequency stable implementation of the even-surface odd-volumetric monopolar-RWG discretization of the EFIE [4], EFIE[tet][Lp-St;o-monoR], where half of the field-contributions are either surface-tested or volumetrically tested. Hence, this impedance matrix cannot be obtained from the algebraic manipulation of the fully volumetric implementation EFIE[tet][monoR]. This is disadvantageous when compared with EFIE[TN][Lp-St;o-monoR], which arises naturally from the algebraic manipulation of EFIE[TN][monoR].
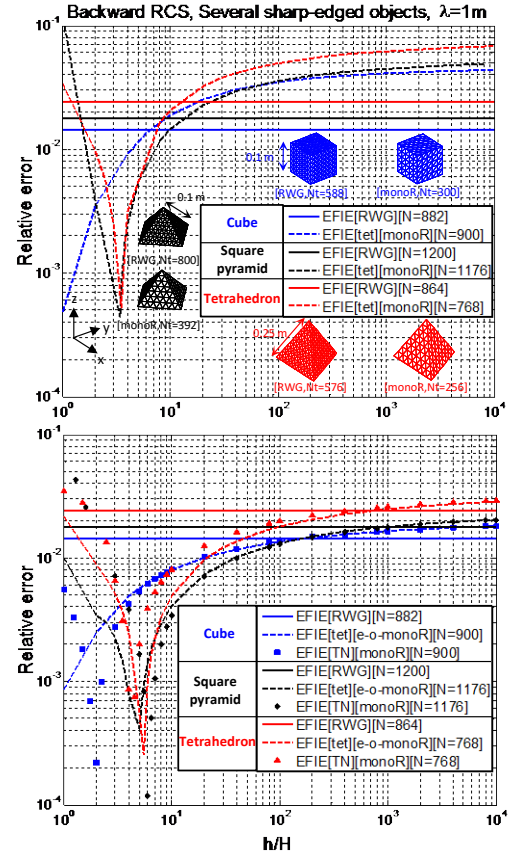
Fig. 4. Relative error for several sharp-edged conductors of the backward scattered RCS versus the height H of the testing elements, defined as a fraction of the mesh parameter h, computed with several monopolar-RWG EFIE-implementations with tetrahedral or tangential-normal testing (λ=1m).

IV. RESULTS

In Figs. 4 and 5, we illustrate the observed improved accuracy of EFIE[TN][monoR] with respect to the RWG-discretization of the EFIE [2], EFIE[RWG], for several closed sharp-edged objects: a cube with side 0.1λ, a square-pyramid with side 0.1λ and a regular tetrahedron with side 0.25λ (λ=1m). The improved accuracy observed for monopolar-RWG implementations is particularly notorious for electrically small sharp-edged objects, because of the important sharp-edge influence on the scattered fields [4]. For the sake of comparison, RCS results for monopolar-RWG discretizations of the EFIE, with tetrahedral volumetric testing [4], are also presented; namely, fully volumetric EFIE[tet][monoR], and even-surface odd-volumetric, EFIE[tet][e-o-monoR]. An x-polarized z-propagating plane wave is impinging on the tested

conductors.

In Fig. 4, we show the relative error of the backward RCS, in terms of the height (H) of the testing elements, which are defined with regard to the edge length at the matching surface facets (h) (see Fig. 1). The root-mean-square RCS error computed in all directions follows roughly the same trend as the backscattering RCS error, which is the dominant for the tested objects. For a fair comparison, the involved formulations handle similar numbers of unknowns (N) but different number of edges (Ne). The adopted triangulations for EFIE[RWG], with $N=Ne$, hence, need to be more finely meshed than the triangulations used for the monopolar-RWG implementations, where $N=2Ne$. The relative errors are referred to RCS-references computed with EFIE[RWG] and extremely fine meshes (around 70000 unknowns) [4]. The observed well-performing H-ranges of EFIE[TN][monoR] for the tested conductors, between h and $h/1000$, are similar to the observed H-ranges of EFIE[tet][e-o-monoR], which turn out much broader than the H-ranges in EFIE[tet][monoR], where the well-performing H-range lies between h and $h/10$ [4][5]. In Fig. 5, the RCS error against the number of unknowns of EFIE[TN][monoR], with $H=h/10$, exhibits a faster speed of convergence than EFIE[RWG], as expected in view of Fig. 4.
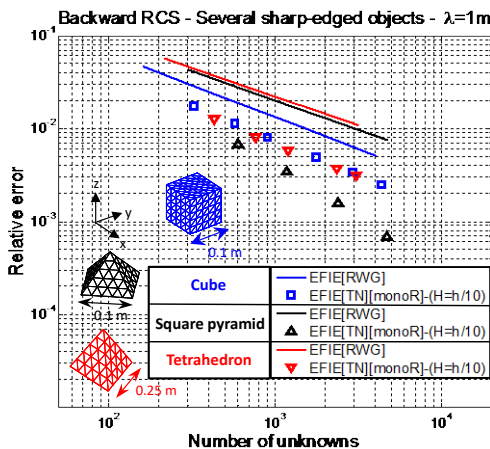
Fig. 5. Relative error of the backward scattered RCS versus the number of unknowns computed with RWG and tangential-normal monopolar-RWG implementations of the EFIE for several sharp-edged objects (λ=1m).

In Fig. 6, we show the RCS for the composite conductor arising from the juxtaposition of a rectangular prism on top of a cube. Two meshes are used with different number of triangles (Nt): a conformal mesh (Nt=1728) and a nonconformal mesh (Nt=1046). The RWG-discretization and the even-surface odd-volumetric monopolar-RWG discretization of the EFIE, edge-oriented, cannot handle the nonconformal mesh because some neighboring triangles have nonmatching edges. In contrast, the tangential-normal or the volumetric monopolar-RWG discretizations of the EFIE, facet oriented, become well suited. In light of Fig. 6, the RCS computed for the nonconformal mesh with EFIE[TN][monoR] and EFIE[tet][monoR] compares well with EFIE[RWG] and the conformal mesh. Moreover, our numerical tests show that the matrix generation for EFIE[TN][monoR] involves half of the time required for EFIE[tet][monoR] (with similar number of quadrature or cubature points). The testing entities in

EFIE[TN][monoR] and EFIE[tet][monoR] are defined so that the information about the edges around each surface facet is ignored because they may be nonmatching with the edges of the adjacent triangles. The inner triangle in the tangential-normal testing is therefore defined normal to the surface triangle and the tetrahedral testing is carried out with right triangular prisms (see Fig. 6).
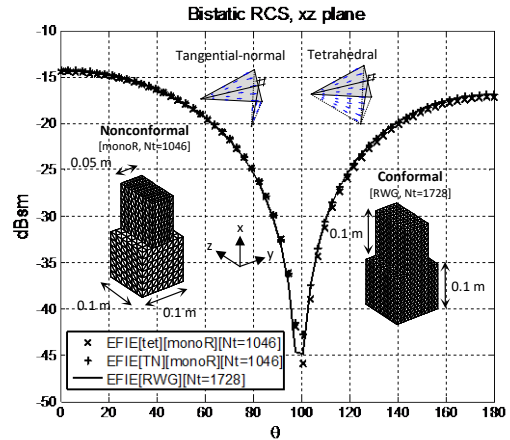
Fig. 6. xz plane cut of the RCS computed with several EFIE-implementations under an impinging x-polarized z-propagating plane wave for an object composed of a rectangular prism on top of a cube. The observation angle θ=0 corresponds with the backscattering direction. Two meshes are used: conformal, with 1728 triangles, or nonconformal, with 1046 triangles (λ=1m).

V. CONCLUSION

The monopolar-RWG EFIE-discretization with tangential-normal testing is amenable to conformal and nonconformal meshes and gives rise to much smaller matrix generation times than the tetrahedral, volumetric or surface-volumetric, implementations. For the moderately small sharp-edged conductors tested, it offers similar RCS-accuracy as the even-surface odd-volumetric implementation. Furthermore, unlike the fully volumetric implementation, it can be set free from the low-frequency breakdown through an algebraic manipulation.

REFERENCES

[1] R. D. Graglia, D. R. Wilton and A. F. Peterson, "Higher Order Interpolatory Vector Bases for Computational Electromagnetics", *IEEE Transactions on Antennas and Propagation*, vol. *45*, No. *3*, pp. *329-342*, March 1997.

[2] S. M. Rao, D. R. Wilton and A. W. Glisson, "Electromagnetic Scattering by surfaces of Arbitrary Shape", *IEEE Transactions on Antennas and Propagation*, vol. *AP-30*, No. *3*, pp. *409-418*, May 1982.

[3] E. Ubeda and J. M. Rius, "Monopolar divergence-conforming and curl-conforming low-order basis functions for the electromagnetic scattering analysis", *Microwave and Optical Technology Letters*, vol. *46*, no. *3*, pp. *237-241*, August 2005.

[4] E. Ubeda, Juan M. Rius and A. Heldring, "Nonconforming discretization of the Electric-Field Integral Equation for closed perfectly conducting objects", *IEEE Transactions on Antennas and Propagation*, vol. *62*, no. *8*, pp. *4171-4186*, August 2014.

[5] E. Ubeda, Juan M. Rius, A. Heldring and I. Sekulic, "Volumetric testing parallel to the boundary surface for a nonconforming discretization of the Electric-Field Integral Equation", *IEEE Transactions on Antennas and Propagation*, vol. *63*, no. *7*, pp. *3286-3291*, July 2015.

[6] J. Zhao and W. C. Chew, "Integral equation solution of Maxwell's equations from zero frequency to microwave frequencies," *IEEE Transactions on Antennas and Propagation*, vol. *48*, no. *10*, pp. *1635-1645*, Oct. 2000.